Chapter 12
Turbulent Flow Due to Moving Continuous Surfaces

The turbulent flow due to moving continuous surfaces is another aspect of the viscous boundary-layers in addition to the laminar flows presented in the previous two parts. The literature on turbulent boundary-layer flows due to the moving (translating) or stretching surfaces is, literally, very few and is strictly limited to the uniformly moving plate and the slim continuous cylinder cases only. These flows were also considered by Sakiadis in his pioneering papers [1, 2] on this topic. In comparison with the laminar flows of this class, the turbulent flows are almost completely unknown to the best of our knowledge. After the historic initiative of Sakiadis, the idea had not been progressed, so far, by the subsequent investigators in the case of turbulent flows. Ultimately, this created a huge gap between the laminar and the turbulent flows of this class. The present chapter focuses particularly on the turbulent flow due to the translating or stretching continuous surfaces. Sakiadis [1, 2] considered the turbulent flow due to a uniformly moving flat plate and a long slim continuous cylinder of constant cross section. In Sect. 12.1, the Sakiadis' turbulent flow in the said two cases is being presented while the Crane's turbulent flow, namely due to the stretching sheet and the stretching cylinder, has been considered in Sect. 12.2. Approximate analytic solution in all the four cases has been obtained due to the integral method approach.

12.1 Turbulent Sakiadis Flow

12.1.1 Two-Dimensional Case

The two-dimensional laminar boundary-layer flow of an incompressible viscous fluid is governed by Eqs. (2.10)–(2.11) (with $w \equiv 0$) where the right-hand side involves the derivative of the laminar shear stress only. In the turbulent two-dimensional flows too, the governing system [Eqs. (2.10)–(2.11)] stays the

A. Mehmood, *Viscous Flows*, Mathematical Engineering,
DOI 10.1007/978-3-319-55432-7_12

same but with a modified right-hand side. The shear stress, of turbulent flow, does not follow the simple Newton's law of viscosity (only) but involves an additional contribution due to the turbulent eddies. The description of such turbulent eddies is not any straightforward and requires their appropriate modeling. Therefore, different describing models for the turbulent Reynolds stresses have been developed, in this regard. The selection of appropriate turbulent model depends strongly upon the nature of flow, under investigation. Based upon empirical data, the turbulent shear stresses have been modeled in terms of physical boundary-layer parameters and such empirical models have their general acceptability having the capacity of producing sufficiently accurate results. Nevertheless, the numerical or theoretical solution of a turbulent flow always requires a comparison with the experiment in order to state a concrete conclusion about the studied particular flow. Unfortunately, the Sakiadis' turbulent flow has never been studied experimentally to the best of our knowledge. Because of this hindrance, it has always been impossible to compare the theoretical results with any experimental data.

The current theoretical analysis compromises of an approximate integral method solution for various power-law velocity profiles. More clear and authentic picture of these flows will stay pending until the availability of experimental data for these flows.

Approximate solution

The momentum integral equation for a two-dimensional Sakiadis flow is given in Eq. (2.26). For laminar flows, the wall shear stress $(\tau_{x,0})$ simply follows the Newton's law of viscosity, whereas, for turbulent flows, it requires appropriate modeling. Based on the Blasius law of friction, the famous so-called wall law of the pipe flow is equally valid for the two-dimensional case also and is given by

$$\tau_{x,0} = \rho V_{\alpha}^2, V_{\alpha} = 0.150 u_w^{7/8} \left(\frac{\nu}{\delta}\right)^{1/8}, \tag{12.1}$$

where V_{α} denotes the friction velocity. The momentum and displacement thicknesses in this case are defined as

$$\theta = \int_0^{\delta} \left(\frac{u}{u_w}\right)^2 \mathrm{d}y, \tag{12.2}$$

and

$$\delta^* = \int_0^{\delta} \frac{u}{u_w} \mathrm{d}y, \tag{12.3}$$

respectively. The momentum integral Eq. (2.26) can also be rewritten in terms of momentum thickness as

$$\frac{\mathrm{d}}{\mathrm{d}x}\left(u_w^2\theta\right) = \frac{\tau_{x,0}}{\rho}. \tag{12.4}$$

Sakiadis utilized the famous power-law velocity profile of the form

$$\frac{u}{u_w} = 1 - \left(\frac{y}{\delta}\right)^{\frac{1}{n}}, \tag{12.5}$$

in his integral method and chose to use the value $n = 7$. The substitution of Eq. (12.5) in momentum integral Eq. (12.4), for $n = 7$, results in a first-order ordinary differential equation in $\delta(x)$, of the form

$$\frac{1}{36}\frac{\mathrm{d}\delta}{\mathrm{d}x} = 0.0225 Re_\delta^{-1/4}, \tag{12.6}$$

where $Re_\delta = \frac{u_w \delta}{\nu}$ is the Reynolds number based on the boundary-layer thickness $\delta(x)$. The integration of Eq. (12.6) yields

$$\frac{\delta}{x} = 1.01002 Re_x^{-1/5}. \tag{12.7}$$

The availability of $\delta(x)$ helps in furnishing the other quantities of interest such as the momentum and displacement thicknesses and the coefficient of wall skin-friction which are calculated as

$$\frac{\theta}{x} = 0.028056 Re_x^{-1/5}, \tag{12.8}$$

$$\frac{\delta^*}{x} = 0.126225 Re_x^{-1/5}, \tag{12.9}$$

and

$$C_f = 0.044890 Re_x^{-1/5}, \tag{12.10}$$

respectively.

It is a generally observed fact that the velocity profile in the turbulent boundary-layer becomes fuller upon increasing the flow Reynolds number. In the same manner, the power-law velocity profile given in Eq. (12.5) becomes fuller upon increasing the power-law index n, such as $n = 8, 9$ or 10. In view of the available experiences with the power-law velocity profile, it has now generally been admitted that the 1/7th power-law profile approximates well for the turbulent Reynolds numbers immediately next to the transition region and gives poor approximation for moderate and higher values of the turbulent Reynolds number. The 1/8th or 1/9th power-law profiles fit quite well to the experimental data for

moderate Reynolds numbers, that is, of the order of 10^7 or 10^8 and the 1/10th power-law profile for the turbulent Reynolds numbers of the order of 10^9 and 10^{10} as is also observed in the case of rotating disk flow. In what follows, the Sakiadis' integral solution seems to be limited to small turbulent Reynolds numbers and requires to be improved for moderate and higher turbulent Reynolds numbers. In this regard, the values 8, 9, and 10 of the power-law index "n" have also been considered and the results for physical quantities of interest have been furnished in the following.

To include the results for other values of n (i.e., $n = 8, 9$ & 10), the general 1/nth power-law profile, given in Eq. (12.5), is utilized. In doing so, Eq. (12.6) modifies as

$$\frac{\mathrm{d}\delta}{\mathrm{d}x} = 0.0225 C_{1/n}^{-1} Re_{\delta}^{-1/4}, \tag{12.11}$$

which integrates to give

$$\frac{\delta}{x} = 0.05745 C_{1/n}^{-4/5} Re_x^{-1/5}, \tag{12.12}$$

where $C_{1/n} = 1 - 2A + B; A = \frac{n}{n+1}, B = \frac{n}{n+2}$. Consequently, Eqs. (12.8)–(12.10) do also modify and, respectively, read as

$$\frac{\theta}{x} = 0.05745 (C_{1/n}^{-1} Re_x)^{-\frac{1}{5}}, \tag{12.13}$$

$$\frac{\delta^*}{x} = 0.05745 \frac{(1-A)}{C_{1/n}} (C_{1/n}^{-1} Re_x)^{-\frac{1}{5}}, \tag{12.14}$$

$$C_f = 0.09192 (C_{1/n}^{-1} Re_x)^{-\frac{1}{5}}, \tag{12.15}$$

The Sakiadis' solution for 1/7th profile is also contained in the results given in Eqs. (12.12)–(12.15) and can readily be recovered by substituting $n = 7$ (see Table 12.1). The above results for 1/nth power-law profile are summarized in Table 12.1 and have also been compared to the case of surface of finite length. The boundary-layer thickness for continuous surface is quite larger than that of surface of finite length. Because of this fact, the coefficient of skin-friction is smaller for continuous surface in comparison with the finite surface. The momentum thicknesses in the two cases are, however, comparable, but the displacement thicknesses of the two cases differ by large from each other.

The velocity curves for $n = 7, 8, 9$ & 10 are plotted in Fig. 12.1 showing that the velocity becomes fuller upon increasing the power-law index n. The boundary-layer, momentum and displacement thicknesses, and the coefficient of skin-friction are plotted in Figs. 12.2, 12.3, 12.4, and 12.5 against the longitudinal

Table 12.1 Comparison between the continuous and the finite surface cases

	$1/n$	$\frac{\delta}{x} Re_x^{1/5}$	$\frac{\theta}{x} Re_x^{1/5}$	$\frac{\delta^*}{x} Re_x^{1/5}$	$C_f Re_x^{1/5}$
Continuous surface	1/7	1.01002	0.0280562	0.1262253	0.0448900
	1/8	1.20742	0.0268317	0.134158	0.0429307
	1/9	1.41769	0.0257761	0.141769	0.0412418
	1/10	1.64031	0.0248531	0.149119	0.0397650
Finite surface	1/7	0.3700	0.0360	0.0460	0.0576
	1/8	0.3983	0.0354	0.0442	0.0566
	1/9	0.4260	0.0350	0.0430	0.0557
	1/10	0.4526	0.0343	0.0411	0.0549

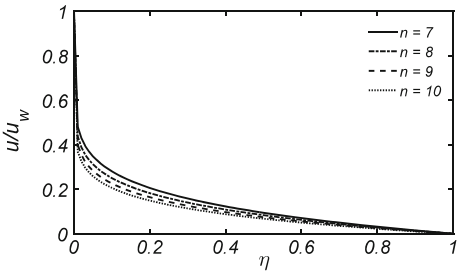

Fig. 12.1 Power-law velocity profile

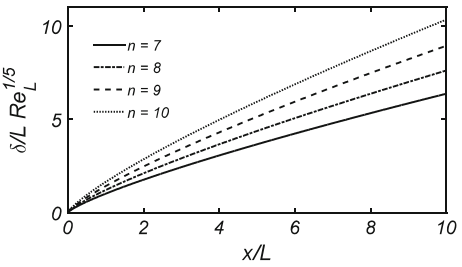

Fig. 12.2 Variation of boundary-layer thickness in x

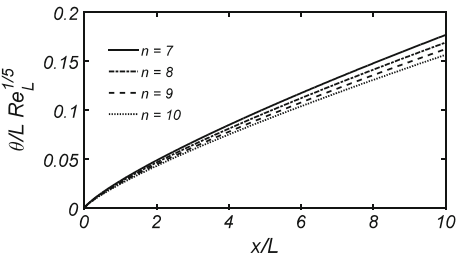

Fig. 12.3 Momentum thickness plotted against x

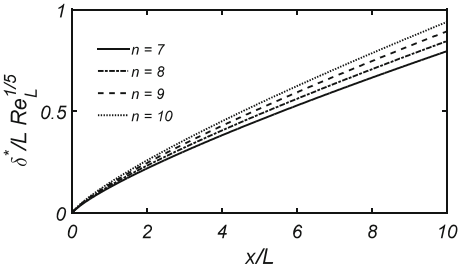

Fig. 12.4 Dependence of displacement thickness upon x

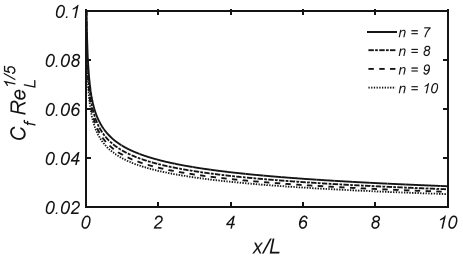

Fig. 12.5 Coefficient of local skin-friction plotted against x

variable x. The three thicknesses, namely the boundary-layer, the momentum, and the displacement ones grow almost linearly as one progresses in the downstream direction.

The consequence of the growing boundary-layer thickness is the decrease in the wall skin-friction coefficient at downstream locations. Furthermore, the momentum thickness decreases and the displacement thickness increases upon increasing the values of n.

12.1.2 The Cylinder Case

The turbulent flow due to a moving continuous cylinder was also investigated by Sakiadis [2] himself with the aid of integral method. He utilized the same 1/7th power-law profile of the continuous flat plate in this case too. Unfortunately, Sakiadis failed in obtaining physically reliable results in this case. However, the method developed by him involves great mathematical beauty and allows a direct comparison with the results of corresponding flat surface case. The momentum integral equation applicable to this case is given in Eq. (2.29) (for a permeable surface), and in the case of impermeable surface, the normal wall velocity must be taken equal to zero, that is, $v_w = 0$. Following the previous case, Eq. (2.29) (with $v_w = 0$) can also be rewritten as

$$\frac{\mathrm{d}}{\mathrm{d}z}\left(u_w^2 R\theta\right) = R\frac{\tau_{z,0}}{\rho}, \tag{12.16}$$

where R denotes the radius of the infinite cylinder and θ denotes the momentum thickness given by

$$\theta = \int_R^\delta \left(\frac{u}{u_w}\right)^2 r\mathrm{d}r,$$

which for the cylinder of constant radius $R = R_0$ reads as

$$\theta = \int_{R_0}^\delta \left(\frac{u}{u_w}\right)^2 r\mathrm{d}r.$$

The momentum area, in this case, is obtained due to the momentum thickness as

$$\Theta = \pi\left[(R_0+\theta)^2 - R_0^2\right].$$

The famous wall law of the pipe flow, given in Eq. (12.1), is assumed to be applicable in this case too for the approximation of wall shear stress. The utilization of the 1/7th power-law profile of the form given in Eq. (12.5) transforms Eq. (12.16) to the form

$$\frac{\mathrm{d}}{\mathrm{d}z}\left[\delta\left(\frac{1}{36}+\frac{1}{120}\frac{\delta}{R_0}\right)\right] = 0.0225\left(\frac{\delta}{z}\right)^{-1/4} Re_z^{-1/4}. \tag{12.17}$$

Integration of above equation results in a nice mathematics which allows a direct comprises between the present case and the case of the corresponding flat continuous surface. Equation (12.17) integrates to give

$$\left[\frac{\delta}{z}\left(1+0.167\frac{\delta}{R_0}\right)\right] = 1.01002\left(\frac{\delta}{z}\right)^{-1/4} Re_z^{-1/4},$$

or

$$\frac{\delta}{R_0} = \lambda\phi^{4/5}, \tag{12.18}$$

where $\phi = \left(\frac{z}{R_0}\right)^{5/4} Re_z^{-1/4}$ and λ comes out to be the ratio of cylinder's boundary-layer thickness to that of the flat-plate case, that is, $\lambda = \delta/\delta_p$. The calculated values of ϕ, due to Eq. (12.18), give the ratio of the boundary-layer thickness of the present case to the flat-plate case. For particularly chosen values of

Table 12.2 Values of λ obtained due to 1/7th power-law profile

$\phi^{\frac{1}{5}}$	λ
0	1.000
0.5	0.987
1.0	0.891
1.5	0.682
2.0	0.500
2.5	0.371
3.0	0.281
3.5	0.220
4.0	0.177
5.0	0.122
6.0	0.088
7.0	0.068

ϕ, the corresponding values of λ are listed in Table 12.2. Contrary to the laminar case, the calculated boundary-layer thickness in the cylinder case comes out to be less thick than that of the flat-plate case (see Table 12.2), which is of course incorrect. In actual, the boundary-layer thickness in the cylinder case is larger than the corresponding flat-plate case because of the presence of surface curvature. This fact has also been observed in the self-similar and non-similar flows on a continuous cylinder in the previous two parts. Such a flaw in the present results forbade one from the further analysis.

The ratio of the surface drag of the two cases, namely the cylinder and the flat plate, is given by

$$\frac{D}{D_p} = \left(1 + 0.152\frac{\delta}{R_0}\right)\phi, \tag{12.19}$$

which is also underpredicted by the present method (see Table 12.3). Sakiadis held responsible, however, partly, to the utilized 1/7th power-law profile for such incorrect results.

The generalization of the Sakiadis' results for the 1/*n*th power-law profile is also obtained by utilizing the general power-law profile given in Eq. (12.5). The momentum integral Eq. (12.16), after the utilization of Eq. (12.5), results in the following form

$$\frac{\mathrm{d}}{\mathrm{d}z}\left[\delta\left(K_1 + \frac{1}{2}K_2\frac{\delta}{R_0}\right)\right] = 0.0225\left(\frac{\delta}{z}\right)^{-1/4} Re_z^{-1/4}, \tag{12.20}$$

where $K_1 = -2(A - B - C), K_2 = AD^{-1} - 4D; C = \frac{B}{n}, D = \frac{n}{2n+1}$.

Integration of Eq. (12.20) again results in the form of ratio of two boundary-layer thicknesses, as before, that is,

Table 12.3 Ratio of the surface drag predicted by 1/7th power-law profile

$\phi^{\frac{1}{5}}$	D/D_p
0	1.00
0.5	1.00
1.0	1.01
1.5	1.05
2.0	1.11
2.5	1.18
3.0	1.25
3.5	1.33
4.0	1.40
5.0	1.54
6.0	1.65
7.0	1.75

$$K_1 \frac{\delta}{z}\left(1+\frac{5}{9}\frac{K_2}{K_1}\frac{\delta}{R_0}\right) = 0.028125\left(\frac{\delta}{z}\right)^{-1/4} Re_z^{-1/4},$$

or

$$\frac{\delta}{R_0} = \lambda_{1/n}\phi^{4/5}, \tag{12.21}$$

where $\lambda_{1/7} \equiv \lambda$. The values of the ratio $\lambda_{1/n}$ are listed in Table 12.4 for different values of ϕ corresponding to various values of the power-law index n. Evidently, the 1/8th,…,1/10th profiles also fail to predict the correct results as the ratio $(\lambda_{1/n})$ quickly becomes less than 1. However, the ratio is observed to stay greater than 1 a little bit longer for greater values of n in comparison with the smaller values of n.

Table 12.4 Summarized results for various values of n in the axisymmetric case

$\phi^{1/5}$	$\lambda_{1/n}$			
	$n = 7$	$n = 8$	$n = 9$	$n = 10$
0.0	1.009988	1.207380	1.417506	1.640247
0.5	1.001619	1.195741	1.401729	1.619465
1.0	0.902676	1.062546	1.227275	1.397360
1.5	0.697155	0.803691	0.909795	1.017103
2.0	0.508408	0.578480	0.647087	0.715591
2.5	0.375222	0.423967	0.471305	0.518745
3.0	0.285203	0.320999	0.355611	0.390268
3.5	0.223301	0.250739	0.277202	0.303691
4.0	0.179422	0.201166	0.222104	0.243059
5.0	0.123252	0.137952	0.152080	0.166218
6.0	0.090121	0.100778	0.111012	0.121252
7.0	0.068961	0.077076	0.084876	0.092655

This indicates the requirement of some major modification in the integral method for the turbulent flow on a continuous cylinder.

12.2 Turbulent Crane's Flow

The turbulent (Crane's) flow due to a stretching continuous surface either in the two-dimensional planer case or axially symmetric case is the subject of this Section. After the Sakiadis' pioneering work, the turbulent flow due to moving continuous surfaces has never been considered to the best of our knowledge. Besides the fundamental nature of these flows, they still require proper attention by the theorists and the experimentalists for their complete understanding and further exploration.

At this point, the author takes the privilege to express that the modern developments in CFD and the commercialization of research have forced the new entering scientists and the engineers to get involved in the commercially sponsored research. Consequently, the topics of fundamental research kept on being ignored with the passage of time and now they have totally become "outdated." Following the engineers, the theorists and more particularly the Mathematicians and the Physicists have also been involved in such a CFD-based research by ignoring the mathematical/theoretical development of the field. With the continued practice of this trend, a time may come when the new generation will totally be unaware of the fundamental topics and tools of research in fluid dynamics. In what follows, the big lose will definitely be borne by the Mathematics. Therefore, this is a time when the competent researchers in the field of fluid dynamics must also spend their efforts on the theoretical research especially on mathematical methods in order to make the new generations well aware of the advanced research bearing a strong connection with its essential fundamental basis. Because of these reasons, the famous Sakiadis and Crane's flows must be given proper attention by the experimentalists as well as theorists in order to develop appropriate theoretical procedures regarding their investigation. The axially symmetric flow of a moving or stretching cylinder, as considered in the previous and the current sections, respectively, reveals the scarce of the availability of the authentic data and thus the handicapping of the theoretical procedures.

In the following, the turbulent viscous flow due to a stretching sheet and a stretching cylinder is considered. The previously utilized integral method has again been employed here by using general power-law velocity profile. The presented results are, however, not any authentic rather misleading in the cylinder case, but nevertheless have been reported for the purpose of motivation.

12.2.1 Stretching Sheet

The turbulent flow due to a stretching sheet is also governed by the same equation [Eq. (2.26)] as utilized in the previous section. The pipe law of friction velocity [Eq. (12.1)] is also assumed applicable here. In view of these assumptions, the momentum integral equation [Eq. (2.26)] after the substitution of self-similar 1/*n*th power-law profile takes the form

$$C_{1/n}\frac{1}{x^2}\frac{\mathrm{d}}{\mathrm{d}x}\left(x^2\delta\right) = 0.0225\,Re_{\delta}^{-1/4}. \tag{12.22}$$

Equation (12.22) admits a solution of the power-law form given by

$$\frac{\delta}{x} = K_{1/n}^{\delta}\,x^{\alpha_e-\frac{3}{5}}\,Re_x^{-1/5}, \tag{12.23}$$

where $K_{1/n}^{\delta}$ and α_e are pure dimensionless constants and are given by

$$K_{1/n}^{\delta} = 0.022375\,C_{1/n}^{-4/5}, \quad \text{and} \quad \alpha_e = \frac{3}{5}. \tag{12.24}$$

Corresponding to various values of n, the values of $K_{1/n}^{\delta}$ are shown in Table 12.5.

Because of these values given in Eq. (12.24), Eq. (12.23) finally furnishes as

$$\frac{\delta}{x} = 0.022375(C_{1/n}^4\,Re_x)^{-\frac{1}{5}}. \tag{12.25}$$

With the aid of Eq. (12.25), the expressions of the momentum and displacement thicknesses and of the wall skin-friction coefficient are furnished as

$$\frac{\theta}{x} = 0.022375(C_{1/n}^{-1}\,Re_x)^{-\frac{1}{5}}, \tag{12.26}$$

$$\frac{\delta^*}{x} = 0.022375(1-A)(C_{1/n}^4\,Re_x)^{-\frac{1}{5}}, \tag{12.27}$$

Table 12.5 Values of the constant coefficient [defined in Eq. (12.24)] for various n in the Crane's flow

1/*n*	$K_{1/n}^{\delta}$	
	Two-dimensional	Axisymmetric
1/7	0.393461	0.320875
1/8	0.47036	0.381278
1/9	0.552268	0.444873
1/10	0.638992	0.511402

Table 12.6 Summarized results for turbulent stretching sheet flow

$1/n$	$\frac{\delta}{x} Re_x^{1/5}$	$\frac{\theta}{x} Re_x^{1/5}$	$\frac{\delta^*}{x} Re_x^{1/5}$	$C_f Re_x^{1/5}$
1/7	0.393461	0.0109295	0.0491827	0.0568182
1/8	0.470360	0.0104524	0.0522622	0.0543382
1/9	0.552268	0.0100412	0.0552268	0.0522006
1/10	0.638992	0.0096817	0.0580902	0.0503314

$$C_f = 0.116345(C_{1/n}^{-1} Re_x)^{-\frac{1}{5}}, \tag{12.28}$$

respectively. The above results are summarized in the form of a Table for various values of n in Table 12.6.

12.2.2 Stretching Cylinder

The case of uniformly stretching cylinder follows similarly as does the case of uniformly translating cylinder considered in the previous Section. After the substitution of $1/n$th power-law velocity profile given in Eq. (12.5), the governing momentum integral equation [Eq. (12.16)], in view of Eq. (12.1), takes the form

$$2K_1\left(1+\frac{1}{2}\frac{z}{\delta}\frac{\mathrm{d}\delta}{\mathrm{d}z}+\frac{1}{2}\frac{z}{R}\frac{\mathrm{d}R}{\mathrm{d}z}\right)+K_2\frac{\delta}{R}\left(1+\frac{z}{\delta}\frac{\mathrm{d}\delta}{\mathrm{d}z}\right)=0.0225\left(\frac{\delta}{z}\right)^{-5/4}Re_z^{-1/4}. \tag{12.29}$$

The above equation follows a solution of the form

$$\frac{\delta}{R_0}=K_{1/n}^{\delta}\left(\frac{z}{R_0}\right)^{m_1}Re_{R_0}^{-1/5}, \tag{12.30}$$

under the restriction that the radius R of the cylinder must also follow the same form as does the boundary-layer thickness, that is,

$$\frac{R}{R_0}=\left(\frac{z}{R_0}\right)^{m_2}Re_{R_0}^{-1/5}. \tag{12.31}$$

The constant $K_{1/n}^{\delta}$ and the exponents m_1 and m_2, appearing in Eqs. (12.30)–(12.31), are pure dimensionless constants. In this case, it is found that $m_1 = m_2 = 3/5$, and $K_{1/n}^{\delta}$satisfies the following equation:

$$K_1+\frac{1}{2}K_2K_{1/n}^{\delta}=0.007031\left(K_{1/n}^{\delta}\right)^{-5/4}. \tag{12.32}$$

Table 12.7 Summarized results for the turbulent stretching cylinder flow

$1/n$	$\frac{\delta}{z} Re_z^{1/5}$	$\frac{\Theta}{\pi z^2} Re_z^{2/5}$	$\frac{\bar{\delta}^*}{\pi z^2} Re_z^{2/5}$	$C_f Re_z^{1/5}$
1/7	0.320875	0.018684	0.087083	0.059790
1/8	0.381278	0.017896	0.093280	0.057267
1/9	0.444873	0.017219	0.099391	0.055100
1/10	0.511402	0.016630	0.1050436	0.053214

The values of $K_{1/n}^{\delta}$ corresponding to different values of n are listed in Table 12.5. Important quantities of physical interest such as the boundary-layer thickness, momentum and displacement areas, and the coefficient of wall skin-friction are given by

$$\frac{\delta}{z} = K_{1/n}^{\delta} Re_z^{-\frac{1}{5}},$$

$$\frac{\Theta}{\pi z^2} = 2\left(K_1 + \frac{1}{2} K_2 K_{1/n}^{\delta}\right) K_{1/n}^{\delta} Re_z^{-\frac{2}{5}},$$

$$\frac{\bar{\delta}^*}{\pi z^2} = \left((2 - 2A) + (1 - 2D) K_{1/n}^{\delta}\right) K_{1/n}^{\delta} Re_z^{-\frac{2}{5}},$$

$$C_f = 0.045 \left(K_{1/n}^{\delta}\right)^{-\frac{1}{4}} Re_z^{-\frac{1}{5}}.$$

Corresponding to the various values of the power-law index n, the results are summarized in Table 12.7.

References

1. B.C. Sakiadis, Boundary-layer behavior on continuous solid surfaces: II the boundary-layer on a continuous flat surface. AIChE **7**(2), 221–225 (1961)
2. B.C. Sakiadis, Boundary-layer behavior on continuous solid surfaces: III the boundary-layer on a continuous cylindrical surface. AIChE **7**(3), 467–472 (1961)